RESEARCH ARTICLE

NANO · MICRO small
www.small-journal.com

Balancing Flexible Side Chains on 2D Conjugated Acceptors Enables High-Performance Organic Solar Cell

Xingqi Bi, Shitong Li, Tengfei He, Hongbin Chen, Yu Li, Xinyuan Jia, Xiangjian Cao, Yaxiao Guo, Yang Yang, Wei Ma, Zhaoyang Yao, Bin Kan, Chenxi Li, Xiangjian Wan, and Yongsheng Chen**

Balancing the rigid backbones and flexible side chains of light-harvesting materials is crucially important to reach optimized intermolecular packing, micromorphology, and thus photovoltaic performance of organic solar cells (OSCs). Herein, based on a distinctive CH-series acceptor platform with 2D conjugation extended backbones, a series of nonfullerene acceptors (CH-6F-Cn) are synthesized by delicately tuning the lengths of flexible side chains from *n*-octyl to *n*-amyl. A systemic investigation has revealed that the variation of the side chain's length can not only modulate intermolecular packing modes and crystallinity but also dramatically improve the micromorphology of the active layer and eventual photovoltaic parameters of OSCs. Consequently, the highest PCE of 18.73% can be achieved by OSCs employing D18:PM6:CH-6F-C8 as light-harvesting materials.

1. Introduction

Organic solar cell (OSC) has unique characteristics such as flexibility, nontoxicity, good transparency, etc.[1–5] Moreover, large-area OSC panels can be manufactured by low-cost solution processing methods, which further improves their commercial feasibility.[6–15] These advantages make their great potential applications that can complement traditional silicon-based photovoltaic cells well.[16–24] In recent years, the power conversion efficiencies (PCEs) of OSCs increased rapidly and have exceeded 19% for single-junction devices.[25–35] Thanks to the extensive exploration of A-D-A type acceptors, their tunable structure and energy levels enable organic photovoltaic devices to achieve the short circuit current (J_{SC}), open circuit voltage (V_{OC}) and fill factor (FF) in a balanced manner to achieve higher PCEs.[36–58]

In 2019, Zou et al. reported a noteworthy molecule, denoted as Y6,[59] featuring an electron-withdrawing benzothiadiazole as the central unit. Since then, numerous modifications have been conducted on the Y6 framework with the aim of fine-tuning intermolecular packing properties and nanoscale morphologies.[29,30,59–62] Notably, much optimization to the side chains has been proven as a crucial factor in achieving better photovoltaic performances of OSCs greatly. For instance, Hou's group has synthesized a series of compounds, namely BTP-eC11, BTP-eC9, and BTP-eC7, by gradually shortening the lengths of the side chain.[60] Among them, BTP-eC9 exhibited exceptional solubility along with improved intermolecular ordering, which makes it one of the best acceptor materials so far.[29] Furthermore, Sun et al. explored an acceptor (L8-BO) by incorporating 2-butyloctyl alkyl chain as side groups, which contributed to OSCs with a remarkable PCE of 18.2% and an excellent FF exceeding 81%.[30] In a similar approach, Yan et al. replaced alkyl side groups with aromatic ones, resulting in a significant enhancement in PCEs.[61] The studies above revealed that delicately tuning side chains on such an excellent Y6 backbone could regulate simultaneously the solubilities, light absorptions, crystallinity, accumulation modes, and phase separations of light-harvesting materials, thus could maximize the resulting photovoltaic performances of OSCs.

Recently, a series of CH-series acceptors have been developed by our group, which are featured with 2D conjugated backbones.[38,63,64] Note that the conjugated extension of CH-series acceptors with respect to that of Y6 could give rise to

X. Bi, S. Li, T. He, H. Chen, Y. Li, X. Jia, X. Cao, Z. Yao, B. Kan, C. Li, X. Wan, Y. Chen
State Key Laboratory of Elemento-Organic Chemistry
The Centre of Nanoscale Science and Technology
Institute of Polymer Chemistry
Tianjin Key Laboratory of functional polymer materials
College of Chemistry
Renewable Energy Conversion and Storage Center (RECAST)
Nankai University
Tianjin 300071, China
E-mail: zyao@nankai.edu.cn; yschen99@nankai.edu.cn

Y. Guo
State Key Laboratory of Separation Membranes and Membrane Processes
School of Chemistry
Tiangong University
Tianjin 300387, China

Y. Yang
The Institute of Seawater Desalination and Multipurpose Utilization
Ministry of Natural Resources (Tianjin)
Tianjin 300192, China

W. Ma
State Key Laboratory for Mechanical Behavior of Materials
Xi'an Jiaotong University
Xi'an 710049, China

The ORCID identification number(s) for the author(s) of this article can be found under https://doi.org/10.1002/smll.202311561

DOI: 10.1002/smll.202311561

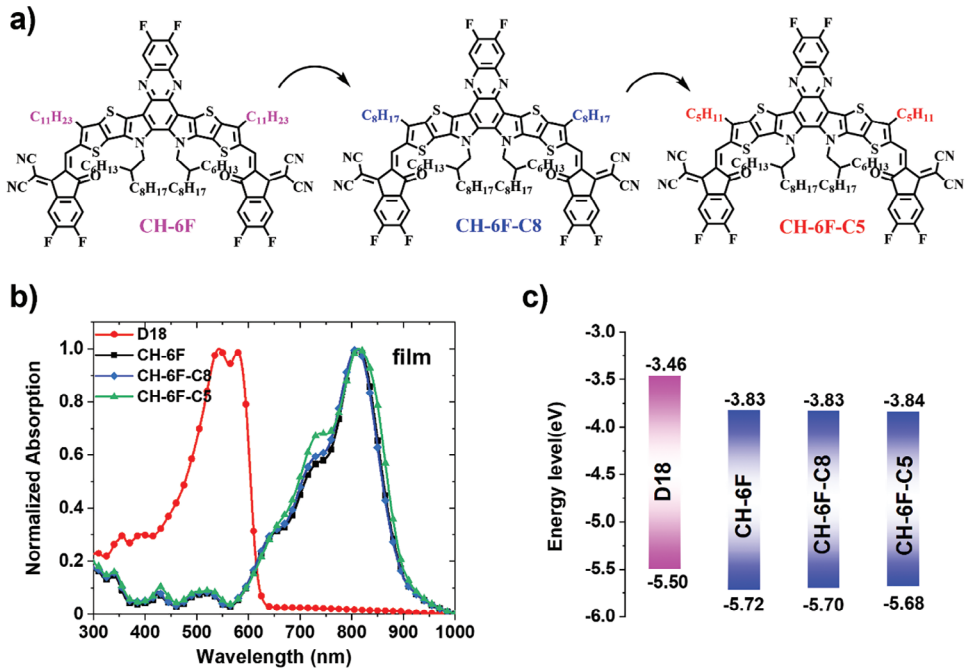

Figure 1. a) Chemical structures of **CH-6F**, **CH-6F-C8,** and **CH-6F-C5**. b) Normalized absorption spectra of neat films. c) Energy levels derived from the CV of neat films.

much enhanced intermolecular actions through more efficient π–π stacking and superior intermolecular packing modes.[63,64] As a result, CH-series acceptors demonstrate smaller exciton binding energies, larger relative dielectric constants, and improved molecular crystalline ordering compared to those of Y6.[65] It would be really exciting that if the evolution pathway of previous successful optimization of side chains on Y6 could be one lesson, CH-series acceptors are very likely to afford a more promising molecular platform capable of reaching record-breaking OSCs, especially when taking their various structural modification possibilities into consideration.[63–67] Based on this, three CH-series molecules of CH-6F, CH-6F-C8, and CH-6F-C5 with different lengths of side chains at the thiophene beta position were constructed (**Figure 1**a). The shortening of side chain length changes the physicochemical properties of acceptors, micromorphology of blended active layers, charge transfer/transport kinetics, and even photovoltaic parameters to some degree. Among them, CH-6F-C8 demonstrates fewer molecular conformations and intermolecular accumulation modes, enhanced molecular packing order, and suppressed non-radiative recombination in photovoltaic devices compared to CH-6F and CH-6F-C5. Thus, OSCs based on D18:CH-6F-C8 reached a PCE up to 18.15% and further increased to 18.73% after adding polymer PM6 as the third component. Our work revealed that for the current highly efficient CH-series materials, although typical 2D conjugated extension of molecular backbone significantly enhances the accumulation between molecules, and even solidifies the micromorphology to a certain extent, the fine regulation of side chains will still have a significant impact on their basic physicochemical properties, aggregation behaviors and even final PCEs of resulting OSCs.

2. Results and Discussions

2.1. Synthesis and Characterization

Compound CH-6F, CH-6F-C8, and CH-6F-C5 were synthesized through a similar method according to the literature[38,63,64] and the detailed procedures and characterizations were deposited in the Supporting Information and Schemes S1–S4 (Supporting Information). The UV–vis spectra of these CH-series acceptors-based films are presented in Figure 1b. The very similar optical bandgaps (E_g^{opt}) of CH-6F, CH-6F-C8, and CH-6F-C5 could be derived from their thin-film onset absorption wavelengths (λ_{onset}) of 897, 896, and 903 nm, being 1.38, 1.38, and 1.37 eV, respectively (Table S1, Supporting Information). The CH-6F-C5 film exhibits a slightly red-shifted absorption, indicating the possible formation of more compact packings in its neat films. Cyclic voltammetry (CV) was employed in order to assess the energy levels of frontier molecular orbital (Figure 1c; Figure S1, Supporting Information). The lowest unoccupied molecular orbital (LUMO) energy levels of CH-6F, CH-6F-C8, and CH-6F-C5 are almost identical, being −3.83, −3.83, and −3.84 eV, respectively. Whereas the highest occupied molecular orbital (HOMO) energy levels gradually move up from −5.72, −5.70 to −5.68 eV. Therefore, the bandgaps decreased slightly with the shortening length of side chains from 1.89, 1.87 to 1.84 eV. The similar but slightly smaller bandgap for CH-6F-C5 with respect to the other two acceptors is roughly consistent with the trend of optical bandgaps.

2.2. Molecular Packing in Single Crystals

Our previous investigations have revealed that even a minor structural change in CH-series acceptors could result in

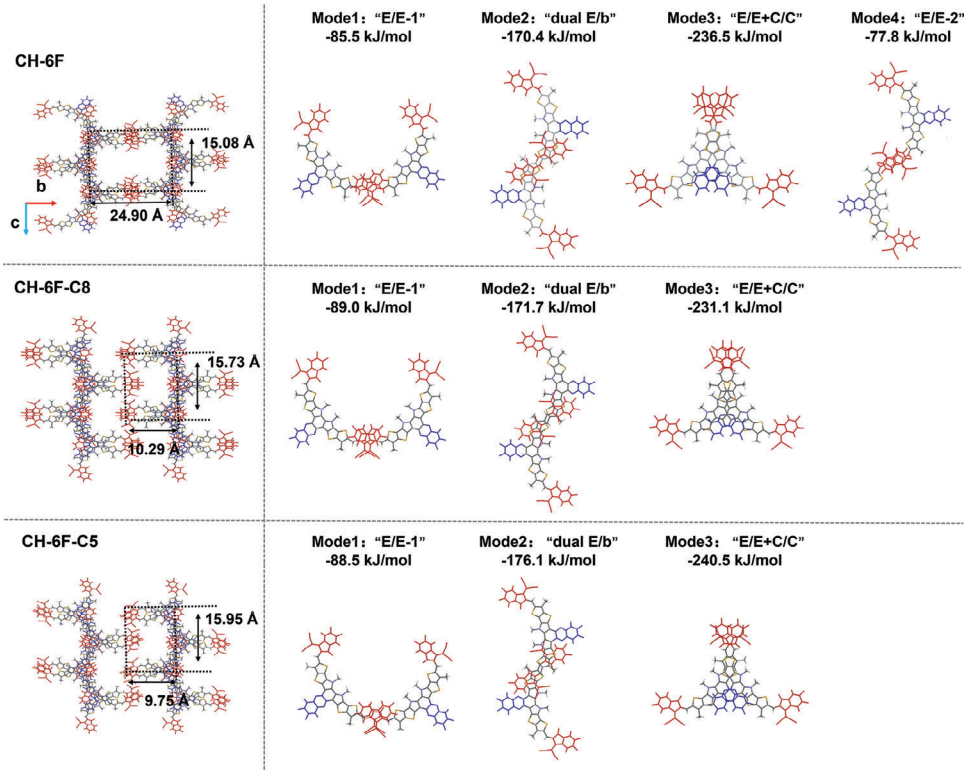

Figure 2. Molecular packing diagrams in single crystals (top view). Red: end unit (E); blue: central unit (C). The packing modes with >|70| kJ mol^{-1} UNI intermolecular potentials were extracted.[68]

significant variation of intermolecular packings and the eventual photovoltaic performance of OSCs.[50] In a similar fashion, the different lengths of side chains may also have a significant influence on the molecular stacking of acceptors. Consequently, single-crystal X-ray diffraction analysis of these CH-series acceptors was conducted to unveil the variation of molecular stacking modes arising from the different side chains. By use of a slow solvent diffusion method with methanol as an antisolvent, needle-like single crystals for CH-series acceptors were obtained in the chloroform phase.[43] The parameters of CH-6F, CH-6F-C8, and CH-6F-C5 single crystals were illustrated in Table S2 (Supporting Information). As displayed in Figure S2 (Supporting Information), all three acceptors are featured with helical molecular geometries and banana-curved profiles. Among them, CH-6F and CH-6F-C5 show two configurations, whereas CH-6F-C8 has only one. The less conformation of CH-6F-C8 may be in favor of forming more ordered molecular stacking and further contribute to much lower energetic disorders.[50] The distances (d_{S-N}) between the N atoms on the phenazine unit and S atoms on adjacent thiophenes are 3.30–3.37 Å, slightly smaller than the sum of their van der Waals radius (≈3.45 Å) and indicative of the possible presence of effective S–N interactions. Note that the efficient S–N interactions provide extra strength to maintain the relatively planar molecular backbones.[32]

As shown in **Figure 2**, different lengths of side chains on 2D-conjugated CH-series acceptors indeed result in different intermolecular stacking modes and 3D molecular packing network structures. For CH-6F, four stacking modes have been identified: Mode 1, referred to as "E/E-1," involves π–π interactions of end units from two molecules. Mode 2 represents distinctive dual-end groups and bridged units' stackings between neighboring molecules (dual E/b). Mode 3 is characterized by tight intermolecular packing involving not only end units but also central cores (E/E+C/C). Additionally, CH-6F also exhibits Mode 4 (E/E-2), which is not presented in CH-6F-C8 and CH-6F-C5 crystals. In the cases of CH-6F-C8 and CH-6F-C5, three similar stacking modes have been observed: "E/E-1," "dual E/b" and "E/E+C/C." Among these, Mode 3 is particularly noteworthy as it has also been observed in highly efficient Y6 and CH series small molecules. Mode 3 exhibits the largest overlap area between neighboring molecules, leading to a substantial enhancement in intermolecular interactions. The corresponding intermolecular stacking potential energy of Mode 3 (−230 to −240 kJ mol^{-1}) is significantly higher compared to those of Mode 1 (−85 to −90 kJ mol^{-1}) and Mode 2 (−170 to −180 kJ mol^{-1}). In addition, the denser molecular accumulations for CH-6F-C8 and CH-6F-C5 may be formed with a much smaller void size of ≈10 * 16 Å than that of ≈25 * 15 Å for CH-6F. It is believed that such reduced pore sizes may facilitate the formation of more efficient 3D charge transport channels.[64]

2.3. Photovoltaic Properties

Different molecular aggregation properties should impact the photovoltaic performances of OSCs. Therefore, OSCs with an architecture of ITO/PEDOT: PSS/Active layer/PNDIT-F3N/Ag (**Figure 3a**) were fabricated. As regards active layers, a polymer

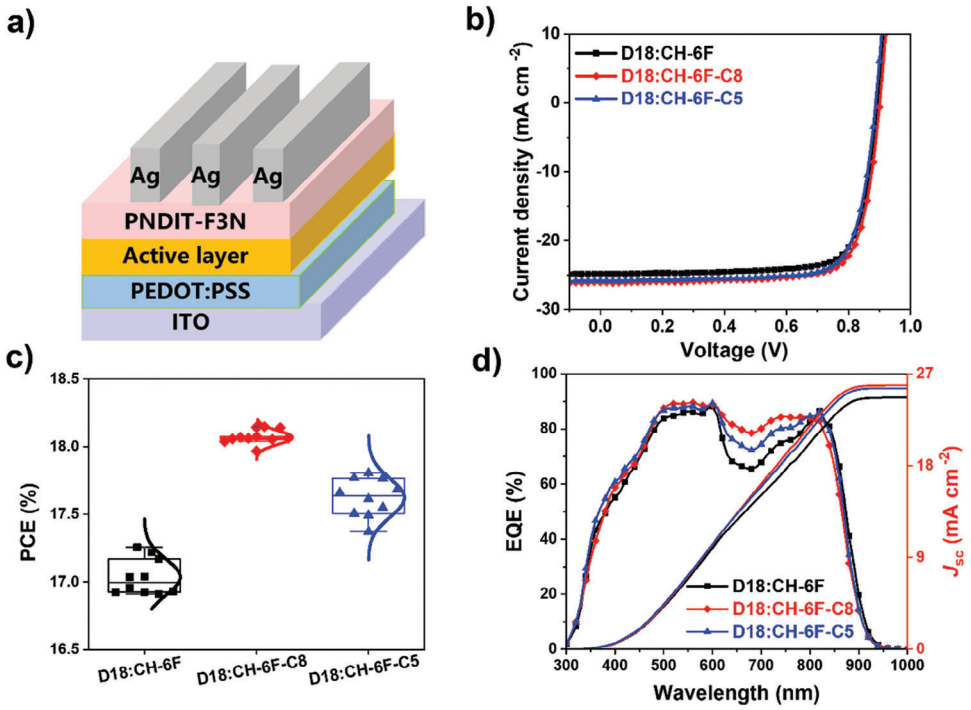

Figure 3. Photovoltaic performances. a) Device structure. b) *J*--*V* curves. c) PCE variations counted by ten devices. d) EQE spectra and integral J_{SC} values.

donor D18[28] with matched energy levels and complementary absorption spectra was selected to blend with CH-6F, CH-6F-C8, and CH-6F-C5 to compose the active layers. As summarized in Tables S3–S8 (Supporting Information), each system has been systematically optimized. The optimal device parameters including *J*–*V* curves for each system are shown in **Table 1** and Figure 3b. The device based on CH-6F-C8 presents an impressive PCE of 18.15% better than that of 17.26% for CH-6F-based devices, along with both excellent J_{SC} of 26.12 mA cm^{-2} and V_{OC} of 0.901 V. CH-6F-C5-based OSCs has slightly lower efficiency of 17.81%, mainly due to their inferior V_{OC} (0.887 V) and J_{SC} (25.81 mA cm^{-2}) compared to those of CH-6F-C8-based one. The efficiency distributions counted by ten devices (Figure 3c) showed excellent device reproducibility for all three acceptors. Note that despite similar bandgaps of CH-6F and CH-6F-C8, a higher V_{OC} of 0.901 V for CH-6F-C8-based OSCs than that of 0.894 V suggests a probably suppressed non-radiative recombination.[69] Besides, considering the importance of device lifespan, the thermal stability of OSCs was preliminarily investigated. As shown in Figure S4 (Supporting Information), after heating all devices at 65 °C for 480 h, the PCEs of CH-6F-, CH-6F-C8-, and CH-6F-C5-based binary OSCs could be maintained above 90% of their initial PCEs.

The external quantum efficiency (EQE) spectra were measured and presented in Figure 3d. The integrated current densities derived from the corresponding EQE plots are 24.68, 25.89, and 25.61 mA cm^{-2} for D18:CH-6F, D18:CH-6F-C8, and D18:CH-6F-C5-based OSCs, respectively. To investigate the reasons for the differences in EQE spectra and J_{SC} of D18:CH-6F, D18:CH-6F-C8, and D18:CH-6F-C5 systems, absorption spectra of blended films were measured. As shown in Figure S5 (Supporting Information), CH-6F-C8 displays slightly larger absorption extinction coefficients than those of CH-6F-C5 and CH-6F. The larger absorption extinction coefficient of CH-6F-C8 is beneficial for utilizing photons, which should partially account for its higher EQEs in OSCs. Then, photo-luminescence (PL) spectra were measured in order to understand the charge transfer processes occurring at the donor and acceptor interface. Figure S6 (Supporting

Table 1. Optimized device performances for D18:CH-6F, D18:CH-6F-C8, D18:CH-6F-C5 and D18:PM6:CH-6F-C8.

Active layer	V_{OC} [V]	J_{SC} [mA cm^{-2}]	J_{SC}^{cal} [mA cm^{-2}]	FF [%]	PCE [%]
D18: CH-6F	0.894 (0.898 ± 0.003)	24.81 (24.43 ± 0.28)	24.68	77.8 (77.6 ± 0.4)	17.26 (17.04 ± 0.13)
D18: CH-6F-C8	0.901 (0.899 ± 0.002)	26.12 (25.96 ± 0.29)	25.89	77.1 (77.4 ± 0.7)	18.15 (18.07 ± 0.05)
D18: CH-6F-C5	0.887 (0.887 ± 0.003)	25.81 (25.58 ± 0.44)	25.61	77.4 (77.5 ± 0.9)	17.81 (17.62 ± 0.14)
D18:PM6: CH-6F-C8	0.888 (0.885 ± 0.002)	26.59 (26.65 ± 0.35)	26.48	79.3 (78.2 ± 0.6)	18.73 (18.43 ± 0.19)

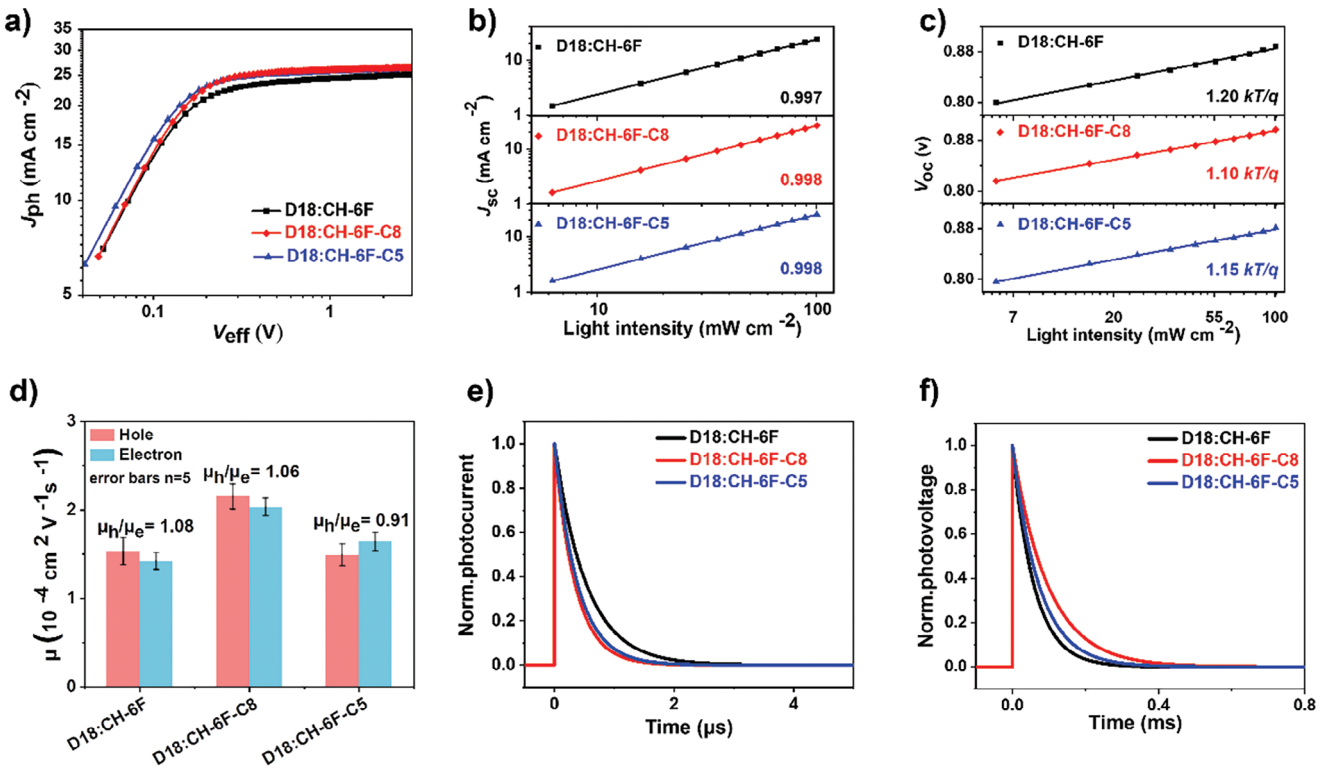

Figure 4. a) J_{ph} versus V_{eff} curves. b) Light intensity (P_{light}) dependence of J_{SC}. c) Light intensity (P_{light}) dependence of V_{OC}. d) Histograms of the electron mobility (μ_e) and hole mobility (μ_h). e) Transient photocurrent measurements. f) Transient photovoltage measurements.

Information) demonstrates that after blending with D18, the film of D18:CH-6F-C8 exhibits the largest PL quenching efficiency of acceptor emission, reaching 96.2%, followed by the D18:CH-6F-C5 film with 90.2% and the D18:CH-6F film with 90.1%, respectively. These results indicate a more efficient charge transfer between the acceptor and D18 in the D18:CH-6F-C8-based blended films and match the highest short-circuit current density obtained by its devices. As shown in **Figure** 4a, measurements of photocurrent density (J_{ph}) versus effective voltage (V_{eff}) were conducted under short-circuit conditions to further gain insights into the charge generation and migration in OSCs. The efficiencies of exciton dissociation (η_{diss}) and charge extraction (η_{coll}) can be obtained by comparing the ratio of J_{ph}/J_{sat} under the short-circuit condition and the maximum power output point, respectively. Here, J_{sat} represents J_{ph} reaching a saturated state. As a result, the D18:CH-6F-C8 device exhibits the highest η_{diss}/η_{coll} (98.75%/89.6%) in comparison with those of D18:CH-6F (97.8%/86.8%) and D18:CH-6F-C5 (98.4%/87.8%) devices, indicating better exciton dissociation and charge collection in D18:CH-6F-C8 devices, which should also account for its highest EQE response.

Subsequently, charge recombination processes of OSCs were further evaluated by measuring the change of J_{SC}/V_{OC} with light intensity (P_{light}). Under different P_{light}, the corresponding J_{SC} follows the equation $J_{SC} \propto (P_{light})^{\alpha}$. The closer the value of α to the unit, the less degree of bimolecular recombination should be suggested.[64] As shown in Figure 4b, the α of the three systems is basically the same and very close to one unit, which is 0.997, 0.998, and 0.997, respectively, indicating that the bimolecular recombination in all three devices is rather low and is not an issue for these devices. Then, the trap-assisted recombination was evaluated by the exponential S in relational $V_{OC} \propto S * \ln(P_{light})$. A value of S closer to kT/q indicates that the trap-assisted recombination is suppressed. Among the three systems, CH-6F-C8-based OSCs have the smallest slope of 1.10 kTq^{-1}, which is significantly lower than that of the D18:CH-6F (1.20 kTq^{-1}) and CH-6F-C5 (1.15 kTq^{-1})-based devices, indicating that the defect-assisted recombination degree in the D18:CH-6F-C8-based devices is the smallest. In Table S12 (Supporting Information), a summary of all relevant parameters has been presented.

The charge mobilities for the hole (μ_h) and electron (μ_e) were measured by employing the space-charge limited current (SCLC) method and illustrated in Figure 4d. D18:CH-6F/D18:CH-6F-C5 exhibits hole mobility of $1.64/1.42 \times 10^{-4}$ and electron mobility of $1.49/1.53 \times 10^{-4}$ cm^2 V^{-1} s^{-1}, respectively. Notably, the devices based on D18:CH-6F-C8 exhibits a hole and electron mobility of 2.03×10^{-4} and 2.15×10^{-4} cm^2 V^{-1} s^{-1}, respectively. Comparatively, the devices based on D18:CH-6F-C8 exhibit the most effective and balanced mobilities when compared to those of D18:CH-6F/D18:CH-6F-C5. This balanced mobility profile is conducive to efficient charge transport and suppressed recombination, leading to an enhanced J_{SC} of OSCs. Moreover, the transient photocurrent and photovoltage (TPC and TPV) decay kinetics of these devices are shown in Figure 4e,f and Figure S7 (Supporting Information). As plotted in Figure 4e, the extraction time based on D18:CH-6F-C8 device is 0.34 μs, slightly smaller than that of D18:CH-6F (0.54 μs) and D18:CH-6F-C5 (0.38 μs), which implies that the charge extraction is very rapid and less charge is

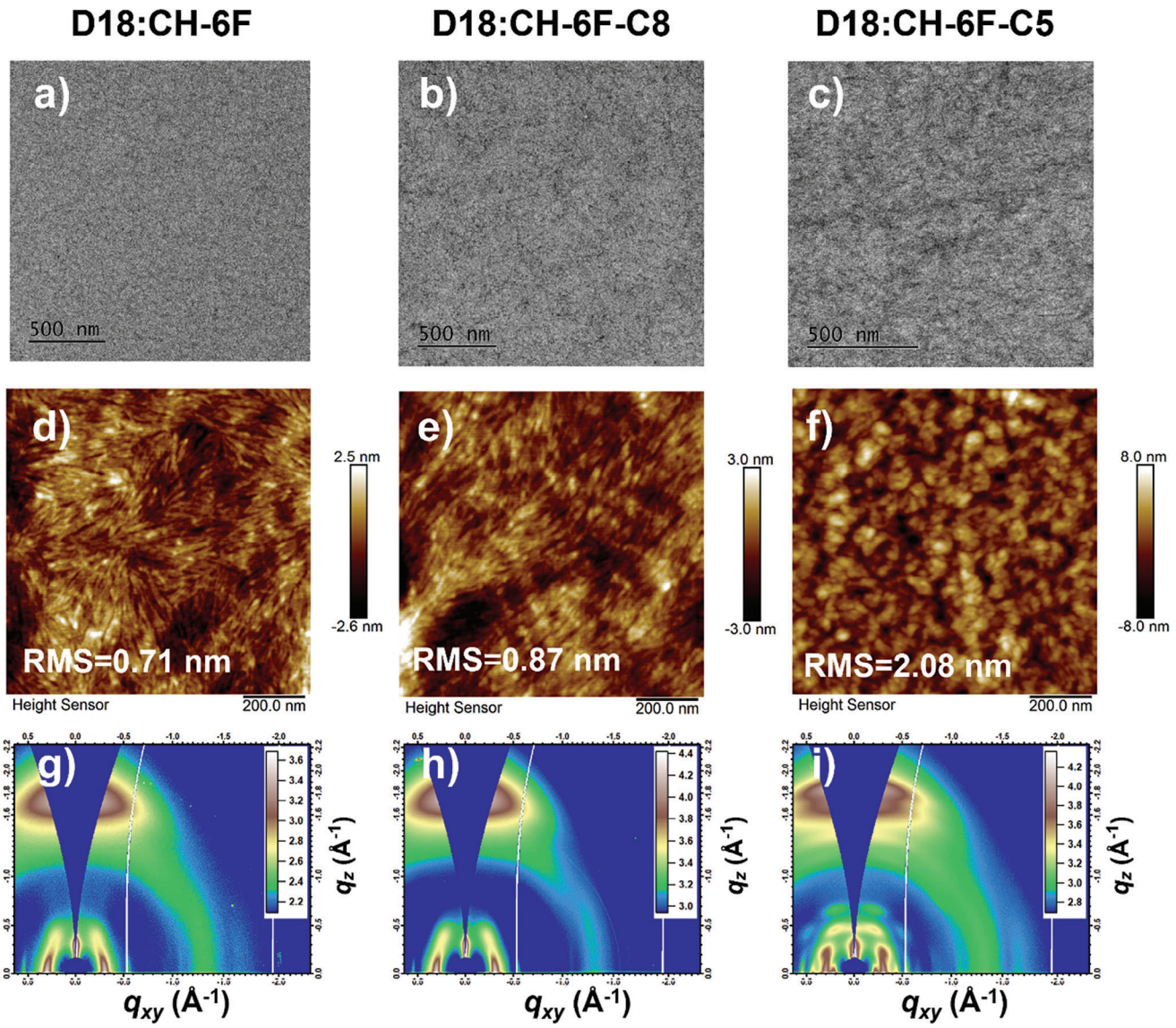

Figure 5. Morphology characterization of blend films. a–c) TEM images. d–f) AFM height images. g–i) 2D GIWAXS patterns of the D18:CH-6F, D18:CH-6F-C8, and D18:CH-6F-C5-based devices.

trapped in D18:CH-6F-C8 based devices. Additionally, the photogenerated carrier lifetime of devices based on D18:CH-6F-C8 is 97 µs according to the TPV characterization (Figure 4f), which is much longer than that of D18:CH-6F (59 µs) and D18:CH-6F-C5 (73 µs). This suggests that the charge recombination process has been suppressed in D18:CH-6F-C8 system, in good accordance with results in above recombination behavior measurements.

In order to achieve a higher PCE for CH-6F-C8-based OSCs, PM6 was selected as the third component.[26,70] Excitingly, D18:PM6:CH-6F-C8-based ternary OSC affords an improved PCE of 18.73%, along with enhanced J_{SC} of 26.48 mA cm^{-2} and FF of 79.3% as collected in Table 1. The *J*–*V* curves and EQE plots of the best devices are displayed in Figure S8 (Supporting Information). As shown in Figure S8 (Supporting Information), the ternary devices have obviously higher EQE values of 600–700 nm. To explain the increase in EQE, absorption spectra of binary and ternary blended films were carried out. As shown in Figure S5b (Supporting Information), ternary blended films exhibit stronger absorption at 600–700 nm, which should come from the absorption of PM6.

2.4. Morphology Analysis

To unveil the influence of the side chain's length on phase separation, we further resorted to transmission electron microscopy (TEM) and atomic force microscopy (AFM). It is clear that the whole film presents a uniform and flat surface in D18:CH-6F blended film from the TEM image (**Figure** 5a). AFM images (Figure 5d,f) further corroborate the flat surface in D18:CH-6F blended films and the root mean square (RMS) of surface roughness is 0.71 nm. The regular fibrous structure can

Table 2. Detailed values for energy losses of OSCs.

Active layer	E_g [eV]	V_{OC} [V]	E_{loss} [eV]	V_{OC}^{SQ} [V]	ΔE_1 [eV]	ΔE_2 [eV]	ΔE_3[a] [eV]	EQE_{EL} [$\times 10^{-4}$]	ΔE_3[b] [eV]
D18:CH-6F	1.418	0.894	0.524	1.154	0.264	0.071	0.189	2.04	0.221
D18:CH-6F-C8	1.420	0.901	0.519	1.157	0.263	0.068	0.188	5.58	0.195
D18:CH-6F-C5	1.421	0.888	0.534	1.158	0.263	0.065	0.205	0.77	0.246

[a] Calculated from V_{OC}^{SQ} through the equation of $\Delta E_3 = V_{OC}^{rad} - qV_{OC}$; [b] Calculated from the EQE_{EL} through the equation of $\Delta E_3 = -kT\ln(EQE_{EL})$.

be seen in the TEM images of D18:CH-6F-C8 blended films (Figure 5b), forming a suitable phase separation scale. Meanwhile, the RMS is slightly increased to 0.87 nm (Figure 5e). D18:CH-6F-C5 blended film shows large-scale phase separation with some large light/dark regions discretely distributed on its TEM images (Figure 5c) and the largest RMS of 2.08 nm can be also obtained (Figure 5f). This rough surface topography may be due to excessive molecular aggregation as the side chains shorten.

To intuitively compare the differences among the three blend films, we have conducted a statistical analysis of nanofiber size (Figure S9, Supporting Information). A gradually increased fiber size can be observed with 8.9 nm for CH-6F 10.4 nm for CH-6F-C8 and 16.6 nm for CH-6F-C5, suggesting that shortening the side chain could enhance molecular crystallinity and enlarge phase domain sizes. As shown in Figure S10 and Table S13 (Supporting Information), $\chi_{D:A}$ for D18: CH-6F-C8 (0.58) and D18:CH-6F-C5 (0.66) are slightly larger than that of D18: CH-6F (0.51), indicating lower D/A miscibility after shortening the side chain of SMAs. This may contribute to the higher domain purity and larger nanofiber size, which is in good accordance with results from AFM and TEM images.

To further comprehend the molecular packing in neat and blended films, grazing incidence wide-angle X-ray scattering (GIWAXS) was carried out. As shown in Figure S11 (Supporting Information), the neat CH-6F, CH-6F-C8, and CH-6F-C5 films exhibit a pronounced (010) peak at ca. 1.73, 1.73 and 1.83 $Å^{-1}$ in out-of-plane (OOP) direction respectively, indicating preferential face-on molecular packing patterns. Note that CH-6F-C5 displays the more prominent (010) diffraction peaks with slightly shifted to larger q values, indicative of a shorter π-π stacking distance of 3.43 Å than those of 3.64 Å for CH-6F and 3.62 Å for CH-6F-C8. In addition, CH-6F-C5 exhibits more diffraction peaks in the out-of-plane direction due to its stronger crystallinity. Meanwhile, In the in-plane (IP) direction, the (100) diffraction peaks of CH-6F, CH-6F-C8, and CH-6F-C5 are located at 0.32, 0.36, and 0.39 $Å^{-1}$, respectively, indicative of gradually decreasing interchain distances of 19.97, 17.68 and 15.99 Å, respectively. As shown in Figure 5g,i, after blending with the D18 donor, the sharp peaks of (010) and (100) diffractions can be still observed in OOP and IP directions, respectively, suggesting that the preferential face-on orientation has been well maintained. As it is summarized in Table S15 (Supporting Information), the (010) diffraction peaks in the OOP direction for three blended films are located at 1.71, 1.72, and 1.83 $Å^{-1}$, corresponding to the π-π stacking distances of 3.67, 3.66, and 3.43 Å, respectively. On the other hand, the interchain stacking distances of D18:CH-6F, D18:CH-6F-C8, and D18:CH-6F-C5 blend films are 20.27, 19.93, and 20.14 Å, respectively.

As the CH-6F side chain shortened to C8, the stacking distance of π–π and the stacking distance between chains were decreased. This enhances the ordering of the active layer. After further shortening the C8 side chain to C5, the phase separation scale of the D18:CH-6F-C5 blend film becomes too large, thus the film becomes non-uniform, and the system may experience significant nonradiative recombination losses. In short, among the three molecules, CH-6F-C8 presents the most suitable stacking, forming obvious fiber-like surface morphologies in the D18:CH-6F-C8 pristine film. This optimized structure is likely to lead to the fewest trap-assisted recombination and improved performance of D18:CH-6F-C8-based devices.(**Table 2**)

2.5. Energy Loss Analysis of OSCs

Herein, we conducted a comprehensive energy loss analysis to quantitatively assess the voltage loss in D18:CH-6F-Cn-based devices. By applying the detailed balance theory, the total E_{loss} was partitioned into three parts, as described below.[71,72]

$$E_{loss} = (E_g - qV_{OC}^{SQ}) + \left(qV_{OC}^{SQ} - qV_{OC}^{rad}\right) + \left(qV_{OC}^{rad} - qV_{OC}\right) = \Delta E_1 + \Delta E_2 + \Delta E_3 \quad (1)$$

The bandgaps (E_g) of blended films, determined by the sensitive EQE (EQE_{PV}) spectra are ≈1.42 eV for all three acceptors. Therefore, the energy loss of the first part (ΔE_1) for three acceptors-based devices is similar (≈0.265 eV). The ΔE_2 is usually defined as additional radiative recombination loss caused by absorption below the bandgap. For D18:CH-6F, D18:CH-6F-C8, and D18:CH-6F-C5 based OSCs, ΔE_2 values were determined to be 0.071, 0.068, and 0.065 eV, respectively. The ΔE_3 is nonradiative energy loss. Herein, D18:CH-6F-C8-based OSCs afford the smallest ΔE_3 of 0.188 eV among the three acceptors, which is further supported by the notably higher external electroluminescence quantum efficiency (EQE_{EL}). Therefore, the higher V_{OC} of the D18:CH-6F-C8-based devices can be attributed to the reduction in radiative and non-radiative recombination losses.[73–75]

3. Conclusion

Three acceptors, CH-6F-Cn (n = 5, 8, and 11), have been designed and synthesized to study the significant effects of flexible side chain lengths on our recently developed 2D conjugated CH-series acceptor platform. A systemic investigation has revealed that CH-6F-C8, with a balanced side chain group, could afford more favorable morphology with a clear and regular nanofiber

structure and moderate π–π stacking distance and inter-chain stacking distance when blended with donor D18 material, thus rendering the device with more efficient exciton dissociation, balanced hole/electron mobility (μ_h/μ_e) and less charge recombination. Thus, a champion PCE of 18.73% of the D18:PM6:CH-6F-C8 system trinary OSCs was achieved. These results indicate that for the current highly efficient CH-series materials, in addition to the already observed significant improvement from the 2D conjugated extension of molecular backbone to their performance, the widely used fine regulation of side chains could also have a great impact on their basic physicochemical properties and even final PCEs. This would clearly offer a promising direction for the further optimization of CH-series materials with already observed high performance.

Supporting Information

Supporting Information is available from the Wiley Online Library or from the author.

Acknowledgements

X.B. and S.L. contributed equally to this work. The authors gratefully acknowledge the financial support from the Ministry of Science and Technology of the People's Republic of China (National Key R&D Program of China, 2022YFB4200400, 2019YFA0705900) and the National Natural Science Foundation of China (21935007, 52025033, 21875182, 21534003). Thanks for the support from Key Scientific and Technological Innovation Team Project of Shaanxi Province (2020TD-002), China Postdoctoral Science Foundation (2017M623162). X-ray data was acquired at beamlines 7.3.3 and 11.0.1.2 at the Advanced Light Source, which is supported by the Director, Office of Science, Office of Basic Energy Sciences, of the U.S. Department of Energy under Contract No. DE-AC02-05CH11231. The authors thank Chenhui Zhu at beamline 7.3.3, and Cheng Wang at beamline 11.0.1.2 for assistance with data acquisition.

Conflict of Interest

The authors declare no conflict of interest.

Data Availability Statement

The data that support the findings of this study are available from the corresponding author upon reasonable request.

Keywords

2D conjugated acceptors, flexible side chains tuning, intermolecular packing, morphology control, organic solar cells

Received: December 20, 2023
Published online:

[1] J. Zhang, H. S. Tan, X. Guo, A. Facchetti, H. Yan, *Nat. Energy* **2018**, *3*, 720.
[2] H. H. Gao, Y. Sun, X. Wan, X. Ke, H. Feng, B. Kan, Y. Wang, Y. Zhang, C. Li, Y. Chen, *Adv. Sci.* **2018**, *5*, 1800307.
[3] H. Chen, H. Lai, Z. Chen, Y. Zhu, H. Wang, L. Han, Y. Zhang, F. He, *Angew. Chem., Int. Ed.* **2021**, *60*, 3238.
[4] R. Ma, C. Yan, J. Yu, T. Liu, H. Liu, Y. Li, J. Chen, Z. Luo, B. Tang, X. Lu, G. Li, H. Yan, *ACS Energy Lett.* **2022**, *7*, 2547.
[5] G. Zeng, W. Chen, X. Chen, Y. Hu, Y. Chen, B. Zhang, H. Chen, W. Sun, Y. Shen, Y. Li, F. Yan, Y. Li, *J. Am. Chem. Soc.* **2022**, *144*, 8658.
[6] Y. Liu, T. P. Russell, *Acc. Chem. Res.* **2022**, *55*, 1097.
[7] Z. Xiao, X. Jia, D. Li, S. Z. Wang, X. J. Geng, F. Liu, J. W. Chen, S. F. Yang, T. P. Russell, L. M. Ding, *Sci. Bull.* **2017**, *62*, 1494.
[8] C.-C. Chueh, C.-Z. Li, A. K. Y. Jen, *Energy Environ. Sci.* **2015**, *8*, 1160.
[9] A. Armin, W. Li, O. J. Sandberg, Z. Xiao, L. M. Ding, J. Nelson, D. Neher, K. Vandewal, S. Shoaee, T. Wang, H. Ade, T. Heumuller, C. Brabec, P. Meredith, *Adv. Energy Mater.* **2021**, *11*, 2003570.
[10] L. J. Zuo, S. H. Zhang, H. Y. Li, H. Z. Chen, *Adv. Mater.* **2015**, *27*, 6983.
[11] L. J. Zuo, C. C. Chueh, Y. X. Xu, K. S. Chen, Y. Zang, C. Z. Li, H. Z. Chen, A. K. Y. Jen, *Adv. Mater.* **2014**, *26*, 6778.
[12] Y. Ma, D. Cai, S. Wan, P. Yin, P. Wang, W. Lin, Q. Zheng, *Natl. Sci. Rev.* **2020**, *7*, 1886.
[13] H. Wang, H. Lu, Y. N. Chen, A. Zhang, Y. Liu, D. Li, Y. Liu, X. Xu, Z. Bo, *Adv. Energy Mater.* **2022**, *12*, 2104028.
[14] Y. Lin, J. Wang, Z. G. Zhang, H. Bai, Y. Li, D. Zhu, X. Zhan, *Adv. Mater.* **2015**, *27*, 1170.
[15] Z. Luo, Y. Gao, H. Lai, Y. Li, Z. Wu, Z. Chen, R. Sun, J. Ren, C. Zhang, F. He, H. Woo, J. Min, C. Yang, *Energy Environ. Sci.* **2022**, *15*, 4601.
[16] X. Xu, L. Yu, H. Meng, L. Dai, H. Yan, R. Li, Q. Peng, *Adv. Funct. Mater.* **2022**, *32*, 2108797.
[17] Y. Wei, Z. Chen, G. Lu, N. Yu, C. Li, J. Gao, X. Gu, X. Hao, G. Lu, Z. Tang, J. Zhang, Z. Wei, X. Zhang, H. Huang, *Adv. Mater.* **2022**, *34*, 2204718.
[18] L. X. Meng, H. Z. Liang, G. K. Song, M. P. Li, Y. Z. Huang, C. Z. Jiang, K. Zhang, F. Huang, Z. Y. Yao, C. X. Li, X. J. Wan, Y. S. Chen, *Sci. China Chem.* **2023**, *66*, 808.
[19] L. Tan, J. Zhou, X. Zhao, S. Wang, M. Li, C. Jiang, H. Li, Y. Zhang, Y. Ye, W. Tress, L. Ding, M. Gratzel, C. Yi, *Adv. Mater.* **2023**, *35*, 2205027.
[20] S. Li, W. Liu, M. Shi, J. Mai, T.-K. Lau, J. Wan, X. Lu, C.-Z. Li, H. Chen, *Energy Environ. Sci.* **2016**, *9*, 604.
[21] Y. Li, X. Huang, K. Ding, H. K. M. Sheriff Jr., L. Ye, H. Liu, C. Z. Li, H. Ade, S. R. Forrest, *Nat. Commun.* **2021**, *12*, 5419.
[22] Y. Cheng, L. Ding, *Energy Environ. Sci.* **2021**, *14*, 3233.
[23] S. Dong, T. Jia, K. Zhang, J. Jing, F. Huang, *Joule* **2020**, *4*, 2004.
[24] H. Ren, Y. Ma, H. M. Liu, J. D. Chen, Y. F. Zhang, H. Y. Hou, Y. Q. Li, Q. Zheng, J. X. Tang, *Adv. Funct. Mater.* **2021**, *32*, 2109735.
[25] K. Chong, X. Xu, H. Meng, J. Xue, L. Yu, W. Ma, Q. Peng, *Adv. Mater.* **2022**, *34*, 2109516.
[26] L. Zhu, M. Zhang, J. Xu, C. Li, J. Yan, G. Zhou, W. Zhong, T. Hao, J. Song, X. Xue, Z. Zhou, R. Zeng, H. Zhu, C.-C. Chen, R. C. I. MacKenzie, Y. Zou, J. Nelson, Y. Zhang, Y. Sun, F. Liu, *Nat. Mater.* **2022**, *21*, 656.
[27] C. He, Y. Pan, Y. Ouyang, Q. Shen, Y. Gao, K. Yan, J. Fang, Y. Chen, C.-Q. Ma, J. Min, C. Zhang, L. Zuo, H. Chen, *Energy Environ. Sci.* **2022**, *15*, 2537.
[28] Q. Liu, Y. Jiang, K. Jin, J. Qin, J. Xu, W. Li, J. Xiong, J. Liu, Z. Xiao, K. Sun, S. Yang, X. Zhang, L. Ding, *Sci. Bull.* **2020**, *65*, 272.
[29] Z. Zheng, J. Wang, P. Bi, J. Ren, Y. Wang, Y. Yang, X. Liu, S. Zhang, J. Hou, *Joule* **2022**, *6*, 171.
[30] C. Li, J. Zhou, J. Song, J. Xu, H. Zhang, X. Zhang, J. Guo, L. Zhu, D. Wei, G. Han, J. Min, Y. Zhang, Z. Xie, Y. Yi, H. Yan, F. Gao, F. Liu, Y. Sun, *Nat. Energy* **2021**, *6*, 605.
[31] M. Zhang, L. Zhu, G. Zhou, T. Hao, C. Qiu, Z. Zhao, Q. Hu, B. W. Larson, H. Zhu, Z. Ma, Z. Tang, W. Feng, Y. Zhang, T. P. Russell, F. Liu, *Nat. Commun.* **2021**, *12*, 309.
[32] R. Sun, Y. Wu, X. Yang, Y. Gao, Z. Chen, K. Li, J. Qiao, T. Wang, J. Guo, C. Liu, X. Hao, H. Zhu, J. Min, *Adv. Mater.* **2022**, *34*, 2110147.

[33] Y. Cui, Y. Xu, H. Yao, P. Bi, L. Hong, J. Zhang, Y. Zu, T. Zhang, J. Qin, J. Ren, Z. Chen, C. He, X. Hao, Z. Wei, J. Hou, *Adv. Mater.* **2021**, *33*, 2102420.
[34] T. Xu, Z. Luo, R. Ma, Z. Chen, T. A. Dela Peña, H. Liu, Q. Wei, M. Li, C. Zhang, J. Wu, X. Lu, G. Li, C. Yang, *Angew. Chem., Int. Ed.* **2023**, *62*, 202304127.
[35] J. Wang, P. Xue, Y. Jiang, Y. Huo, X. Zhan, *Nat. Rev. Chem.* **2022**, *6*, 614.
[36] G. Dennler, M. C. Scharber, C. J. Brabec, *Adv. Mater.* **2009**, *21*, 1323.
[37] L. Meng, Y. Zhang, X. Wan, C. Li, X. Zhang, Y. Wang, X. Ke, Z. Xiao, L. Ding, R. Xia, H.-L. Yip, Y. Cao, Y. Chen, *Science* **2018**, *361*, 1094.
[38] H. Chen, Y. Zou, H. Liang, T. He, X. Xu, Y. Zhang, Z. Ma, J. Wang, M. Zhang, Q. Li, C. Li, G. Long, X. Wan, Z. Yao, Y. Chen, *Sci. China Chem.* **2022**, *65*, 1362.
[39] F. Liu, L. Zhou, W. Liu, Z. Zhou, Q. Yue, W. Zheng, R. Sun, W. Liu, S. Xu, H. Fan, L. Feng, Y. Yi, W. Zhang, X. Zhu, *Adv. Mater.* **2021**, *33*, 2100830.
[40] W. Gao, F. Qi, Z. Peng, F. R. Lin, K. Jiang, C. Zhong, W. Kaminsky, Z. Guan, C. S. Lee, T. J. Marks, H. Ade, A. K. Jen, *Adv. Mater.* **2022**, *34*, 2202089.
[41] X. K. Chen, D. P. Qian, Y. M. Wang, T. Kirchartz, W. Tress, H. F. Yao, J. Yuan, M. Hulsbeck, M. J. Zhang, Y. P. Zou, Y. M. Sun, Y. F. Li, J. H. Hou, O. Inganas, V. Coropceanu, J. L. Bredas, F. Gao, *Nat. Energy* **2021**, *6*, 799.
[42] X. K. Chen, T. H. Wang, J. L. Bredas, *Adv. Energy Mater.* **2017**, *7*, 1602713.
[43] G. Zhang, X. K. Chen, J. Xiao, P. C. Y. Chow, M. Ren, G. Kupgan, X. Jiao, C. C. S. Chan, X. Du, R. Xia, Z. Chen, J. Yuan, Y. Zhang, S. Zhang, Y. Liu, Y. Zou, H. Yan, K. S. Wong, V. Coropceanu, N. Li, C. J. Brabec, J. L. Bredas, H. L. Yip, Y. Cao, *Nat. Commun.* **2020**, *11*, 3943.
[44] W. Liu, S. Li, J. Huang, S. Yang, J. Chen, L. Zuo, M. Shi, X. Zhan, C. Z. Li, H. Chen, *Adv. Mater.* **2016**, *28*, 9729.
[45] A. Rao, P. C. Y. Chow, S. Gelinas, C. W. Schlenker, C.-Z. Li, H.-L. Yip, A. K. Y. Jen, D. S. Ginger, R. H. Friend, *Nature* **2013**, *500*, 435.
[46] L. Zhan, S. Li, T.-K. Lau, Y. Cui, X. Lu, M. Shi, C.-Z. Li, H. Li, J. Hou, H. Chen, *Energy Environ. Sci.* **2020**, *13*, 635.
[47] C. Zuo, L. Ding, *Nanoscale* **2014**, *6*, 9935.
[48] C. Zuo, L. Ding, *Small* **2015**, *11*, 5528.
[49] L. J. Zuo, X. L. Shi, S. B. Jo, Y. Liu, F. Lin, A. K. Y. Jen, *Adv. Mater.* **2018**, *30*, 1706816.
[50] Y. Ma, D. Cai, S. Wan, P. Wang, J. Wang, Q. Zheng, *Angew. Chem., Int. Ed.* **2020**, *132*, 21811.
[51] R. Zhao, N. Wang, Y. Yu, J. Liu, *Chem. Mater.* **2020**, *32*, 1308.
[52] J. Miao, B. Meng, Z. Ding, J. Liu, L. Wang, *J. Mater. Chem. A* **2020**, *8*, 10983.
[53] J. Miao, H. Li, T. Wang, Y. Han, J. Liu, L. Wang, *J. Mater. Chem. A* **2020**, *8*, 20998.
[54] C. Dong, S. Deng, B. Meng, J. Liu, L. Wang, *Angew. Chem., Int. Ed.* **2021**, *133*, 16320.
[55] W. Wang, R. Sun, J. Guo, J. Guo, J. Min, *Angew. Chem., Int. Ed.* **2019**, *58*, 14556.
[56] Y. Shao, Y. Gao, R. Sun, M. Zhang, J. Min, *Adv. Mater.* **2022**, *35*, 2208750.
[57] J. Yao, B. Qiu, Z.-G. Zhang, L. Xue, R. Wang, C. Zhang, S. Chen, Q. Zhou, C. Sun, C. Yang, M. Xiao, L. Meng, Y. Li, *Nat. Commun.* **2020**, *11*, 2726.
[58] Z. Yao, X. Liao, K. Gao, F. Lin, X. Xu, X. Shi, L. Zuo, F. Liu, Y. Chen, A. K. Jen, *J. Am. Chem. Soc.* **2018**, *140*, 2054.
[59] J. Yuan, Y. Zhang, L. Zhou, G. Zhang, H.-L. Yip, T.-K. Lau, X. Lu, C. Zhu, H. Peng, P. A. Johnson, M. Leclerc, Y. Cao, J. Ulanski, Y. Li, Y. Zou, *Joule* **2019**, *3*, 1140.
[60] Y. Cui, H. F. Yao, J. Q. Zhang, K. H. Xian, T. Zhang, L. Hong, Y. M. Wang, Y. Xu, K. Q. Ma, C. B. An, C. He, Z. X. Wei, F. Gao, J. H. Hou, *Adv. Mater.* **2020**, *32*, 1908205.
[61] J. Q. Zhang, F. J. Bai, I. Angunawela, X. Y. Xu, S. W. Luo, C. Li, G. D. Chai, H. Yu, Y. Z. Chen, H. W. Hu, Z. F. Ma, H. Ade, H. Yan, *Adv. Energy Mater.* **2021**, *11*, 2102596.
[62] L. Wang, C. Guo, X. Zhang, S. Cheng, D. Li, J. Cai, C. Chen, Y. Fu, J. Zhou, H. Qin, D. Liu, T. Wang, *Chem. Mater.* **2021**, *33*, 8854.
[63] H. Chen, H. Liang, Z. Guo, Y. Zhu, Z. Zhang, Z. Li, X. Cao, H. Wang, W. Feng, Y. Zou, L. Meng, X. Xu, K. Bin, C. Li, Z. Yao, X. Wan, Z. Ma, Y. Chen, *Angew. Chem., Int. Ed.* **2022**, *61*, 202209580.
[64] Y. Zou, H. Chen, X. Bi, X. Xu, H. Wang, M. Lin, Z. Ma, M. Zhang, C. Li, X. Wan, G. Long, Y. Zhaoyang, Y. Chen, *Energy Environ. Sci.* **2022**, *15*, 3519.
[65] H. Liang, X. Bi, H. Chen, T. He, Y. Lin, Y. Zhang, K. Ma, W. Feng, Z. Ma, G. Long, C. Li, B. Kan, H. Zhang, O. A. Rakitin, X. Wan, Z. Yao, Y. Chen, *Nat. Commun.* **2023**, *14*, 4707.
[66] D. Joly, M. Godfroy, L. Pellejà, Y. Kervella, P. Maldivi, S. Narbey, F. Oswald, E. Palomares, R. Demadrille, *J. Mater. Chem. A* **2017**, *5*, 6122.
[67] Z. Li, B. Zhou, S. Zhang, C. Jiang, Y. Zou, S. Li, Y. Yang, Z. Yao, X. Wan, Y. Chen, *J. Mater. Chem. A* **2023**, *11*, 700.
[68] A. Gavezzotti, G. Filippini, *J. Phys. Chem.* **1994**, *98*, 4831.
[69] D. Qian, Z. Zheng, H. Yao, W. Tress, T. R. Hopper, S. Chen, S. Li, J. Liu, S. Chen, J. Zhang, X.-K. Liu, B. Gao, L. Ouyang, Y. Jin, G. Pozina, I. A. Buyanova, W. M. Chen, O. Inganas, V. Coropceanu, J.-L. Bredas, H. Yan, J. Hou, F. Zhang, A. A. Bakulin, F. Gao, *Nat. Mater.* **2018**, *17*, 703.
[70] M. Zhang, X. Guo, W. Ma, H. Ade, J. Hou, *Adv. Mater.* **2015**, *27*, 4655.
[71] W. Feng, S. Wu, H. Chen, L. Meng, F. Huang, H. Liang, J. Zhang, Z. Wei, X. Wan, C. Li, Z. Yao, Y. Chen, *Adv. Energy Mater.* **2022**, *12*, 2104060.
[72] U. Rau, B. Blank, T. C. M. Muller, T. Kirchartz, *Phys. Rev. Appl.* **2017**, *7*, 044016.
[73] X. Yan, J. Wu, J. Lv, L. Zhang, R. Zhang, X. Guo, M. Zhang, *J. Mater. Chem. A* **2022**, *10*, 15605.
[74] J. Yuan, H. Zhang, R. Zhang, Y. Wang, J. Hou, M. Leclerc, X. Zhan, F. Huang, F. Gao, Y. Zou, Y. Li, *Chem* **2020**, *6*, 2147.
[75] Y. Sun, H.-H. Gao, S. Wu, L. Meng, X. Wan, M. Li, Z. Ma, Z. Guo, S. Li, H. Zhang, C. Li, Y. Chen, *Sci. China Chem.* **2021**, *64*, 608.